Synthesis of Nanocrystalline $BaCeO_3$ by Oxalate Coprecipitation for $YBa_2Cu_3O_7$ Bulk Superconductors

R. Verbová*, V. Kavečanský, P. Diko and V. Antal
Institute of Experimental Physics, Slovak Academy of Sciences, Watsonova 47, Košice, Slovakia

(Received March 31, 2017; in final form November 27, 2017)

Barium cerate ($BaCeO_3$) is one of the preferred additions to bulk $YBa_2Cu_3O_7$ single-grain superconductors to inhibit the growth of Y_2BaCuO_5 particles. The present paper investigates synthesis of very fine barium cerate powder and its use in $YBa_2Cu_3O_7$ bulk superconductor growth. The crystalline barium cerate was synthesized by oxalate co-precipitation from barium and cerium nitrates. X-ray diffraction in air and vacuum was performed to understand the formation of barium cerate as well as to determinate its crystal structure. Size and shape of $BaCeO_3$ particles were studied by scanning electron microscopy. The $BaCeO_3$ was used to grow $YBa_2Cu_3O_7$ bulk superconductor. Microstructure of prepared $YBa_2Cu_3O_7$ crystal shows that the barium cerate in the final product is very fine and uniformly distributed throughout the whole $YBa_2Cu_3O_7$ crystal.

DOI: 10.12693/APhysPolA.133.82
PACS/topics:

1. Introduction

Barium cerate has many possibilities of use in chemistry, one of which is an inhibitor of Y_2BaCuO_5 (Y211) particles growth [1] during fabrication of $YBa_2Cu_3O_7$ (YBCO) bulk single-grain superconductors (BSS). The Y211 particles are very important microstructural elements in YBCO BSS because they provide effective pinning of magnetic flux lines [2]. Since the critical current density, J_c, of the YBCO BSS is directly proportional to the volume fraction of Y211 particles and indirectly to their size, it is necessary to inhibit the growth of Y211 particles [3, 4]. It has been shown that Pt and Ce additions are effective inhibitors of Y211 particles growth [5, 6]. In practice, the addition of Ce is preferred, mainly because of its lower price. Cerium can be added in two forms and these are CeO_2 and $BaCeO_3$. In both cases the powder addition is dissolved in the peritectic melt and inhibits the Y211 particles growth by the Ostwald ripening process [7]. Disadvantage of using CeO_2 is appearance of CuO in the final product due to reaction

$$2\text{Y123} + 3\text{CeO}_2 \Rightarrow 3\text{BaCeO}_3 + \text{Y211} + 5\text{CuO}. \quad (1)$$

It results in a critical concentration of copper oxide, which stops the growth of Y123 crystal [7–9]. It has been also shown that addition of $BaCeO_3$ refines Y211 particles more effectively than CeO_2 [10], but $BaCeO_3$ prepared by solid state reaction often leads to appearance of agglomerates of $BaCeO_3$ in the grown YBCO BSS. Our aim was to prepare very fine barium cerate powder, which would be uniformly distributed throughout the whole volume of the YBCO BSS product.

2. Experimental procedure

Synthesis of barium cerate was inspired by the synthesis described by Vinokurov et al. [11]. This synthesis proceeds in two steps. The first step is preparation of oxalate precursor and the second one is its calcination. The oxalate precursor was prepared by the oxalate co-precipitation method from barium and cerium nitrates. As a co-precipitant ammonium oxalate was used. During stirring to the water/ethyl alcohol (4:1) solution of ammonium oxalate at 80°C, an aqueous solution of barium and cerium nitrates was added, which caused the instant formation of a white precipitate.

The precipitate — oxalate precursor — was filtered and air dried. As mentioned above, the second step is calcination of the precursor. As we wanted to study reactions going on during the synthesis from precursor to barium cerate, the calcination was executed in the high-temperature chamber of X-ray diffractometer (powder diffractometer Rigaku Ultima IV, Cu $K_{\alpha 1,\alpha 2}$ radiation) at $T = 25{-}1100\,^{\circ}\text{C}$ both in air and vacuum ($\approx 2 \times 10^{-3}$ mbar). The X-ray diffraction (XRD) patterns were taken at selected temperatures. The rate of heating was 10 °C/min. The average size of coherent regions was determined from the XRD patterns by the Halder–Wagner methods [12], where LaB_6 from NIST (SRM 660b) was used as a standard reference material. The prepared $BaCeO_3$ powder, in amount corresponding to 1 wt% CeO_2, was added to starting charge of powders with nominal composition $Y_{1.5}Ba_2Cu_3O_x$. After mixing, milling in a friction mill and pressing into cylindrical pellets of 20 mm in diameter, YBCO BSS was fabricated by the top seeded melt growth (TSMG) process [13, 14]. Both the size and shape of $BaCeO_3$ crystallites, as well as microstructure of YBCO crystal were studied by scanning electron microscopy (SEM) by MIRA3 TESCAN microscope. Thermogravimetry measurement (TG) was executed by NETZSCH STA 449 F1 Jupiter.

3. Results and discussion

As mentioned above, the first step was preparation of oxalate precursor, whose XRD pattern and SEM image are depicted in Fig. 1a and b. As can be seen, the average

*corresponding author; e-mail: verbova@saske.sk

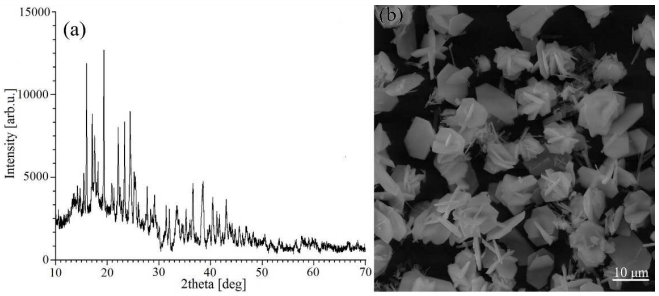

Fig. 1. XRD pattern (a) and SEM image (b) of oxalate precursor.

size of platelet particles in small agglomerates is about 10 μm.

The second step was calcination of oxalate precursor. Our aim was to prepare nanoparticles of barium cerate, therefore the first calcinations were carried out up to 950 °C, both in air and vacuum. The calcination in vacuum was executed because of a lower partial pressure of generated gases over the sample, which could lead to formation of barium cerate phase at a lower temperature, with potentially smaller particles. The resulting XRD patterns of calcination both in air and vacuum are illustrated in Fig. 2a and b, respectively.

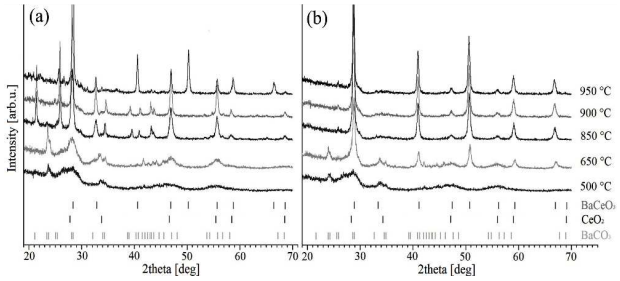

Fig. 2. XRD patterns of calcination of oxalate precursor at $T = 500-950$ °C both in air (a) and vacuum (b).

As seen in the XRD patterns measured at 500 °C, the removing of organic components finished as was also confirmed by the results of thermogravimetry measurement (Fig. 3). At the same time, new phases, barium carbonate and cerium oxide, started to form. In air (Fig. 2a), the powder calcined at 650 °C was a mixture of the phases $BaCO_3$ and CeO_2. The perovskite structure of barium cerate appeared at 950 °C. A different course of reactions was seen in the calcinations in vacuum (Fig. 2b), where the perovskite structure of barium cerate started to form at 650 °C and became clearly dominant at 850 °C.

X-ray powder diffraction of the samples calcined at 950 °C, both in air and vacuum, revealed that these samples were not fully single-phase. It seems that reactions between barium carbonate and cerium oxide were not complete. This assumption was confirmed by the results of thermogravimetry presented in Fig. 3 showing that decrease in weight finished at 1100 °C.

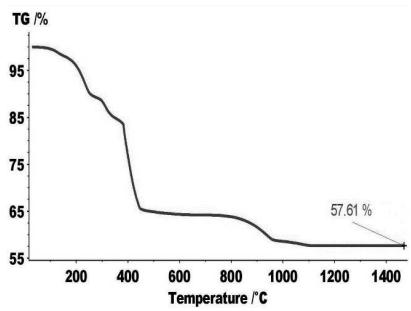

Fig. 3. Thermogravimetry measurements (TG) of oxalate precursor in air, heating rate 15 °C/min.

This stepwise weight decrease can be associated with a complex decomposition of barium carbonate. Several studies [15–17] found that decomposition of $BaCO_3$ took place in three steps with the participation of intermediate phases such as barium oxycarbonate and terminated at a temperature above 1000 °C. Therefore, the next calcinations were performed in a high-temperature chamber up to 1100 °C, both in air and vacuum.

Figure 4 shows the resulting XRD patterns measured at $T = 950-1100$ °C, both in air and vacuum. Only small changes in diffraction patterns can be observed, which proves practically a single-phase barium cerate.

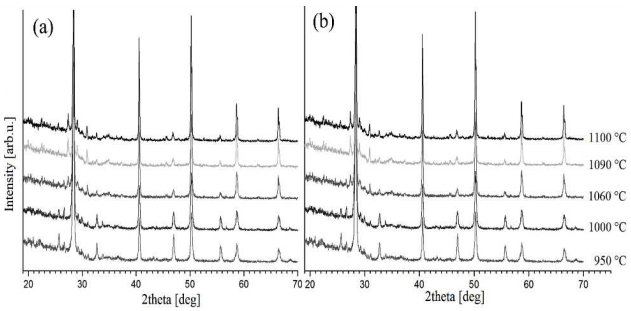

Fig. 4. XRD patterns of calcination of oxalate precursor at $T = 950-1100$ °C both in air (a) and vacuum (b).

Diffraction patterns of samples calcined at 1100 °C, both in air and vacuum, are depicted in Fig. 5. LeBail refinement [18, 19] confirmed match of the measured data with the structural model of barium cerate in orthorhombic symmetry with space group *Pnma*.

Besides the qualitative phase analyses, also the quantitative phase analyses of $BaCeO_3$ phase were performed by RIR method [20]. The quantitative proportion of barium cerate phase in the product is depicted in Fig. 6. It can be seen that calcinations made in vacuum led to formation of $BaCeO_3$ at lower temperatures and nearly 100% $BaCeO_3$ was achieved above 1050 °C.

All calcined samples were also studied by scanning electron microscope. SEM analysis of samples calcined at 950 °C shows that the size as well as the shape of particles after thermal treatment is very similar to the size and shape of particles of oxalate precursor (Fig. 7).

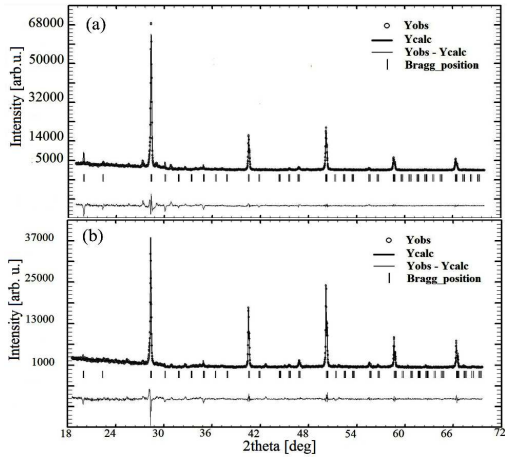

Fig. 5. XRD pattern of barium cerate calcined at 1100 °C both in air (a) and vacuum (b), LeBail refinement.

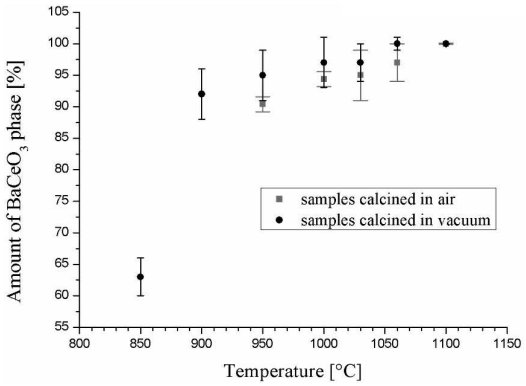

Fig. 6. Temperature dependence of quantitative proportion of $BaCeO_3$ phase [%] determined in samples calcined both in air and vacuum.

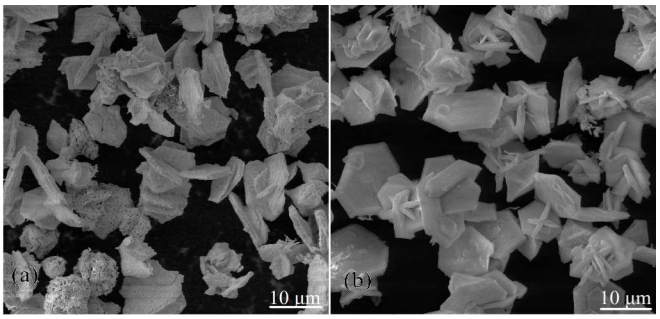

Fig. 7. SEM images of samples calcined at 950 °C both in air (a) and vacuum (b).

The average size of barium cerate particles was about 10 μm. Further, we examined the size of coherent regions of barium cerate from the XRD patterns by the Halder–Wagner method [12]. The resulting values are listed in Table I and graphically illustrated in Fig. 8. The average size of coherent regions was in the range of tens of nanometers.

TABLE I

The average size of coherent regions of barium cerate samples prepared in air and vacuum, determined from XRD patterns by Halder–Wagner method [12].

Temperature [°C]	Average size of coherent regions [nm]	
	calcined in air	calcined in vacuum
850	–	21±1
900	–	22±1
950	38±3	28±1
1000	41±3	37±2
1060	51±2	54±2
1100	68±9	60±4

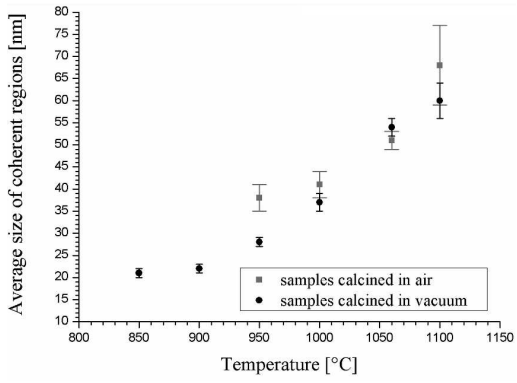

Fig. 8. Temperature dependence of average size of coherent regions of $BaCeO_3$ phase determined in samples calcined both in air and vacuum.

The same trend was also observed in the samples calcined at 1100 °C. Taking this into account, we suppose that the crystallites of barium cerate arise within the initial particles of the oxalate precursor as it is also confirmed by SEM image of the particle surface at higher magnification, where small nanoscale crystallites can be seen (Fig. 9).

According to these results, we prepared barium cerate in such a way that oxalate precursor was calcined in tubular furnace in a moderate vacuum (700 mbar) with dwell 2 h (with temperature rising at the heating rate 100 °C/h up to the temperature of calcination). Thus prepared powder was added to the nominal mixture of powders. The distribution of crystallites in the grown YBCO BSS is presented in Fig. 10.

As can be seen, crystallites of barium cerate were fine and uniformly distributed throughout the whole volume of the sample. This observation confirmed that large brittle $BaCeO_3$ polycrystalline particles were crushed during the milling process of powder mixture and homogeneously distributed in the pressed powder sample and in the final grown YBCO BSS, as well.

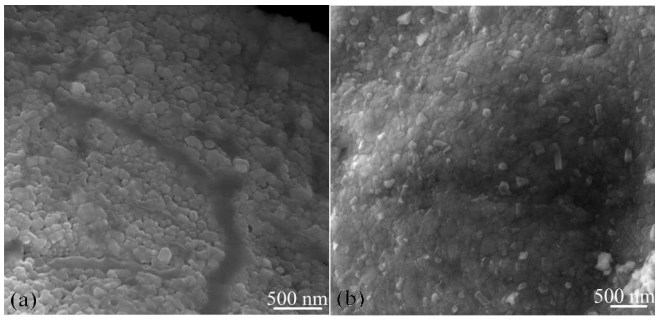

Fig. 9. SEM images of samples calcined at 1100 °C both in air (a) and vacuum (b), focused on the particle surface at higher magnification.

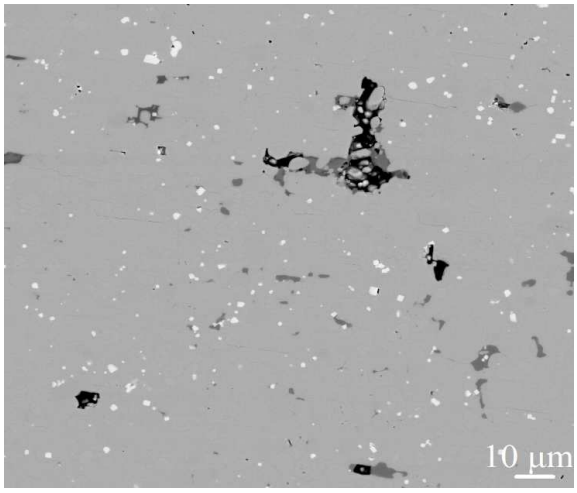

Fig. 10. SEM image of YBCO crystal. The white places are crystallites of barium cerate.

4. Conclusions

Results of oxalate precursor calcination show that the calcination in vacuum leads to formation of barium cerate at lower temperatures with lower size of coherent regions of barium cerate phase.

Studying the samples using scanning electron microscope provided another important information, namely that the particles of barium cerate were very similar to the particles of the oxalate precursor, both in the size and shape, but the size of $BaCeO_3$ coherent regions was in tens of nanometers. By virtue of this fact we suppose that very fine particles of barium cerate arise within the initial particles of oxalate precursor.

We successfully synthesized pure $BaCeO_3$ from the oxalate precursor in vacuum in the form of polycrystalline particles. Addition of this powder led to homogeneously distributed fine $BaCeO_3$ crystallites in the YBCO BSS.

Acknowledgments

This work was realized within the framework of the projects: New Materials and Technologies for Energetic (ITMS 26220220061), Research and Development of Second Generation YBCO Bulk Superconductors (ITMS 26220220041), APVV No. 0330-12, VEGA No. 2/0121/16.

References

[1] P. Diko, D. Volochová, M. Radušovská, K. Zmorayová, M. Šefčíková, V. Antal, K. Jurek, M. Jirsa, J. Kováč, *Physica C* **494**, 31 (2013).

[2] M. Murakami, *Mod. Phys. Lett. B* **4**, 163 (1990).

[3] M. Murakami, K. Yamakuchi, H. Fujimoto, N. Nakamura, T. Taguchi, N. Koshizuka, S. Tanaka, *Cryogenics* **32**, 930 (1992).

[4] K. Nakazato, M. Muralidhary N. Koshizuka, K. Inoue, M. Murakami, *Physica C* **504**, 4 (2014).

[5] C.J. Kim, K.B. Kim, I.H. Kuk, G.W. Hong, *Physica C* **281**, 244 (1997).

[6] C.J. Kim, K.B. Kim, G.W. Hong, *Physica C* **232**, 163 (1994).

[7] P. Diko, M. Šefčíková, M. Kaňuchová, K. Zmorayová, *Mater. Sci. Eng. B* **151**, 7 (2008).

[8] D. Volochová, P. Diko, V. Antal, M. Radušovská, S. Piovarči, *J. Cryst. Growth* **356,** 75 (2012).

[9] D. Volochová, P. Diko, M. Radušovská, S. Piovarči, V. Antal, K. Zmorayová, M. Šefčíková, *J. Supercond. Novel Magn.* **26**, 885 (2013).

[10] K. Zmorayová, M. Šefčíková, D. Volochová, M. Radušovská, V Antal, S. Piovarči, P. Diko, *Phys. Proced.* **45**, 53 (2013).

[11] A.L. Vinokurov, O.A. Shkzajhtin, Y.-O. Oh, A.V. Orlov, Y.D. Tretyakov, *Supercond. Sci. Technol.* **16**, 416 (2003).

[12] N.C. Halder, C.N.J. Wagner, *Acta Crystallogr.* **20**, 312 (1969).

[13] H.C. Li, W.S. Fan, B.N. Peng, W. Wang, Y.F. Zhuang, L.S. Guo, X. Yao, H. Ikuta, *Cryst. Growth Des.* **15**, 1740 (2015).

[14] D.K. Namburi, Y. Shi, K.G. Palmer, A.R. Dennis, J.H. Durrell, D.A. Cardwell, *Supercond. Sci. Technol.* **29**, 095010 (2016).

[15] D. Medvedev, A. Muraskina, E. Pikalova, A. Demin, A. Podias, P. Tsiakaras, *Prog. Mater. Sci.* **60**, 72 (2014).

[16] F. Chen, O.T. Sorensen, G. Meng, D. Peng, *J. Therm. Anal.* **53**, 397 (1998).

[17] F. Chen, O.T. Sorensen, G. Meng, D. Peng, *Solid State Ion.* **100**, 63 (1997).

[18] V.K. Pecharsky, P.Y. Zavalij, *Fundamentals of Powder Diffraction and Structural Characterization of Materials*, Kluwer Academic, USA 2003.

[19] W.I.F. David, K. Shankland, L.B. McCusker, Ch. Baelrocher, *Structure Determination from Powder Diffraction Data*, Oxford University Press, USA 2002.

[20] R.L. Snyder, *Powder Diffr.* **7**, 186 (1992).